Chinese Chemical Letters 34 (2023) 107896

Contents lists available at ScienceDirect

Chinese Chemical Letters

journal homepage: www.elsevier.com/locate/cclet

Hierarchical structures, surface morphology and mechanical elasticity of lamellar crystals dominated by halogen effects☆

Chuanxin Wei[a,b,1], Jianfeng Wang[a,1], Yanni Zhang[a], Xuehua Ding[a], Yanze Jiang[a], Qiang Zhao[a,b], Jinyi Lin[a,*], Jianfeng Zhao[a,*], Linghai Xie[b,*], Wei Huang[a,b,c,*]

[a] Key Laboratory of Flexible Electronics (KLOFE), Institute of Advanced Materials (IAM), Nanjing Tech University (NanjingTech), Nanjing 211816, China
[b] Key Laboratory for Organic Electronics and Information Displays, Institute of Advanced Materials (IAM), Nanjing University of Posts & Telecommunications, Nanjing 210023, China
[c] Institute of Flexible Electronics (IFE), Northwestern Polytechnical University (NPU), Xi'an 710072, China

ARTICLE INFO

Article history:
Received 31 August 2022
Revised 26 September 2022
Accepted 12 October 2022
Available online 17 October 2022

Keywords:
Halogen
Lamellar crystal
Elasticity
Crystal energy framework (CEF)
Inter/intralayer interaction energy (Inter/Intra-IE)

ABSTRACT

To understand the deformation mechanism of molecular crystals under mechanical forces will accelerate the molecular design and preparation of deformable crystals. Herein, the relationship between structural halogenation and molecular-level stacking, micro/nanoscale surface morphology, and macroscopic mechanical properties are investigated. Elastic crystals of halo-pyrimidinyl carbazoles (CzM-Cl, CzM-Br and CzM-I) with lamellar structure and brittle crystal (CzM-F) were quantitatively analyzed by crystal energy framework (CEF) providing the inter/intralayer interaction energy (Inter/Intra-IE). It is revealed that the elastic crystals bend under external force as a result from stronger Intra-IE to prevent cleavage and weaker Inter-IE for the short-range movement of molecules on the slip plane. This research will provide an insight for the molecular design of flexible crystals and facilitate the development of next-generation smart crystal materials.

Organic flexible crystals have been widely focused, including with drug preparation [1–3], flexible optical waveguides [4–8], smart materials [9], laser media materials [10,11], polarization rotors [12,13], hybrid actuators [14–16], mechanical discoloration/mechanochromism [17,18], anti-counterfeiting [19], mechanophotonics [20], and optoelectronic devices [21–25]. Dynamic physical cross-linked structures in crystals is a key factor to realize energy absorption and release, and further ensure the excellent bendable property. An atomic-resolved structural perturbation in the hierarchical structures of elastic crystals is the fundamental molecular landscape to observe under external stimuli including mechanical stress [26,27], light activation [28,29], and thermal annealing [30,31]. The inter/intralayer in the crystal respond to external energy determine the mechanical properties [32,33], which govern these dynamic stress-strain response processes [34]. Similar to hierarchical structures of soft materials, a unique electronic environment in organic molecule is an original factor to modulate the type, intensity and direction of intermolecular non-covalent interactions at different levels in crystal [35–37]. These interactions precisely dominate the intermolecular arrangement within the intralayer of the elastic crystal and exhibit the interlayer structure to realize the energy absorption and release [35]. Therefore, rational molecular designs for pursuing the synergistic effect of hierarchical structures that govern structural perturbation and lamellar structure in the elastic crystal are essential.

Ubiquitous and dynamic non-covalent interaction is fundamental factor to obtain reversible deformation of elastic molecular crystals. The elastic crystal will realize energy absorption and release by structural perturbation, which requires dynamic reversible noncovalent physical crosslinking [27,35,38]. Organic crystals containing halogen atoms are fashionable, such as hexahalogenated benzene crystals [39] and halogenated Schiff base crystals [40] with mechanically deformable behaviors, suggesting their excellent capacity of energy absorption [41]. However, there is a serious debate about the origin of this mechanical flexibility of organic molecular crystals, such as anisotropic packing [42–45] and isotropic packing for plastic and elastic behaviors [38,41,46,47]. Relatively stronger intralayer and weaker interlayer interactions [48] are empirically proved as a precondition of building reversible stress-strain center in hierarchical structures of flexible crystals

☆ Celebrate the 10th anniversary of the Institute of Advanced Materials (IAM) of Nanjing Tech University.

* Corresponding authors.
E-mail addresses: iamjylin@njtech.edu.cn (J. Lin), iamjfzhao@njtech.edu.cn (J. Zhao), iamlhxie@njupt.edu.cn (L. Xie), iamwhuang@njtech.edu.cn (W. Huang).

[1] These authors contributed equally to this work.

https://doi.org/10.1016/j.cclet.2022.107896
1001-8417/

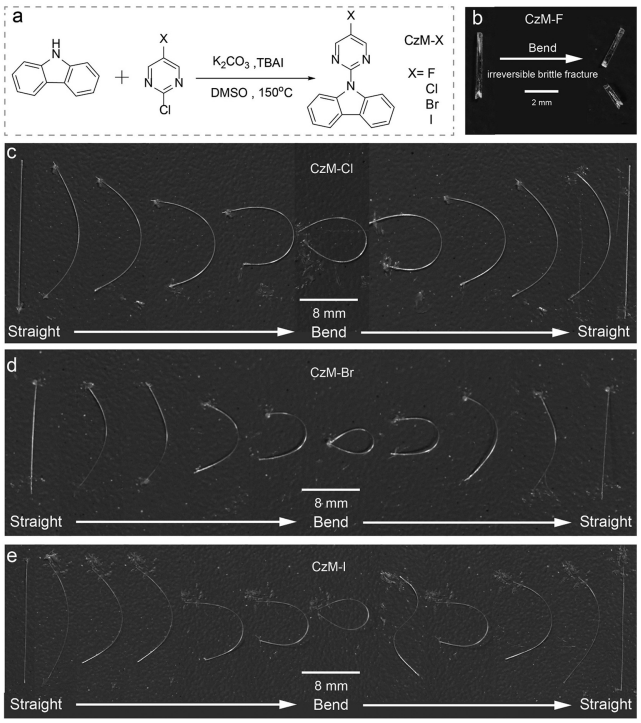

Fig. 1. Materials preparation and images of mechanical response of crystals. (a) Synthetic route of compound CzM-X. The "frozen" bending and recovery states of (b) CzM-F, (c) CzM-Cl, (d) CzM-Br and (e) CzM-I crystals. A general procedure was operated that one end of the needle crystal was fixed, and the opposite end was applied by external force and then fixed by silicon grease with acupuncture needle.

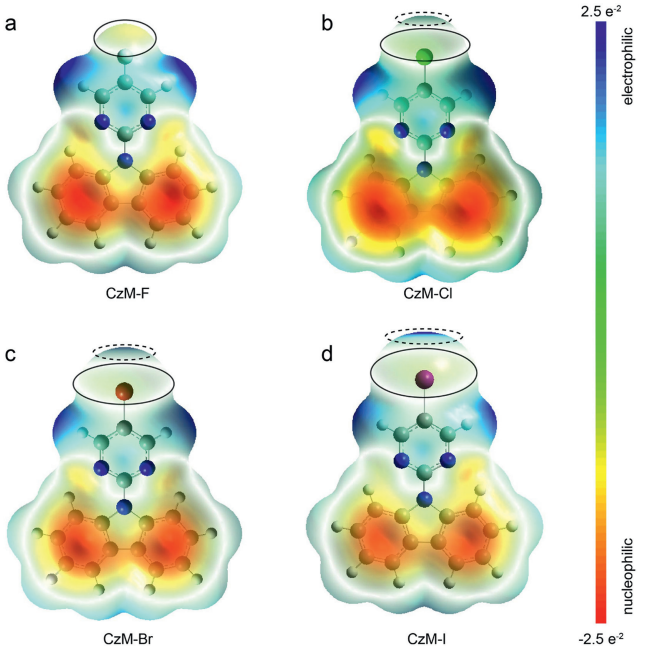

Fig. 2. The electrostatic potential of four single molecules under stable configuration of four halo-pyrimidinyl Cz derivatives. (a) CzM-F (b), CzM-Cl (c) CzM-Br and (d) CzM-I. Solid line section: Electron-rich and high nucleophilic ability. Dotted line section: Electron-deficient and high electrophilic ability.

[35,36]. However, there is a lack of specific quantitative parameters in atomic scale to effectively support the theory that flexible crystals require relatively stronger intralayer and weaker interlayer interactions, which is extremely important to precisely tune intermolecular arrangement toward exploring novel molecular flexible crystal *via* rational molecular design. Herein, we prepared a series of halogen-contained four brittle or elastic crystals with micro/nanoscale with lamellar morphology from halo-pyrimidinyl carbazole (Cz) derivatives (CzM-X: CzM-F, CzM-Cl, CzM-Br and CzM-I) to systematically explore the halogen effects and confirm the theory. The mysterious elasticity was unraveled in the perspective of quantitative inter/intralayer interaction energy (Inter/Intra-IE) and the changes in the micro/nanostructures with crystal deformation *via* scanning electron microscope (SEM) and atomic force microscope (AFM). Although four molecules have similar molecular configurations, conformations and stacking modes in crystals, the C-X bonds (C-F, C-Cl, C-Br and C-I) with different surface potentials on halogen atoms affect the crystal structures which also bring out the mechanical response characteristics of the crystals. The mechanical properties were quantified by nanoindentation. Finally, not only the relationship between the molecular stacking modes and the quantitative Inter/Intra-IE of the elastic lamellar crystals using the crystal energy framework (CEF) [49] were revealed but also the elastic bending mechanism of elastic crystals was reasonably proposed.

CzM-X derivatives, including CzM-F [50], CzM-Cl and CzM-Br [51] and CzM-I were successfully synthesized according to the route shown in Fig. 1a as an improved procedure compared to the literature.[50] Detailed information can be found in Figs. S1–S10 (Supporting information). As shown in Fig. 1b, the CzM-F crystal exhibits brittle nature with irreversible damage and fracture under strong external force. Interestingly, three kinds of crystals exhibited impressive elasticity, and could be bent into the droplet shape (Figs. 1c–e) [51]. When the external force was removed, the straight crystal recovered to original state. This bending-recovery process could be repeated many times and the crystal exhibited macroscopic integrity. Remarkably, the straight CzM-I crystal presented an "S" shape after bending into a drop shape and recovered. The mechanical properties of CzM-F, CzM-Cl, CzM-Br and CzM-I crystals were further quantified by nanoindentation measurement (Fig. S11 in Supporting information). The hardness H and elastic modulus E of these crystals with average values of CzM-F ($H = 0.277$ GPa, $E = 7.77$ GPa), CzM-Cl ($H = 0.237$ GPa, $E = 5.02$ GPa), CzM-Br ($H = 0.211$ GPa, $E = 5.84$ GPa) and CzM-I ($H = 0.369$ GPa, $E = 7.18$ GPa).

The electrostatic potentials of individual molecules from single crystal data were investigated to uncover the different arrangement of four crystals (Gauss software: B3LYP functional and def2-SVP basis set). The electrostatic potentials are almostly similar, in which the large π ring of Cz units are red inside but cyan outside (Fig. 2). The pyrimidine units are cyan and blue. Besides, the surface of the F atom is all red, indicating a nucleophilic behavior (solid line section) (Fig. 2a). However, the surfaces of the Cl, Br and I atoms are partially red (solid line section), and gradually blue (dotted line section) simultaneously showing nucleophilic and electrophilic behaviors (Figs. 2b–d). These slight differences of the electrostatic potential are attributed to the electronegativity of halogen atoms with different radius in C-X bonds (C-F = 1.350 Å, C-Cl = 1.736 Å, C-Br = 1.882 Å, and C-I = 2.098 Å) (Fig. S13 in Supporting information). Therefore, various halogen atoms cause the electron distribution in halogen surface of C-X bond, which also modulate intermolecular non-covalent interaction and arrangements in crystal structures.

Subsequently, the crystals of CzM-F, CzM-Br and CzM-I grow along the *c*-axis. And the crystal of CzM-Cl grows along the *a*-axis, as displayed in Fig. 3 [51]. In addition, the (010) face as the bending face was determined to be the maximum plane of CzM-Cl (Fig. 3e), CzM-Br (Fig. 3h) and CzM-I (Fig. 3k) (Figs. S14 and S15 in Supporting information). The CzM-F molecules along *c*-axis are stacked in parallel by intermolecular $\pi\cdots\pi$ interac-

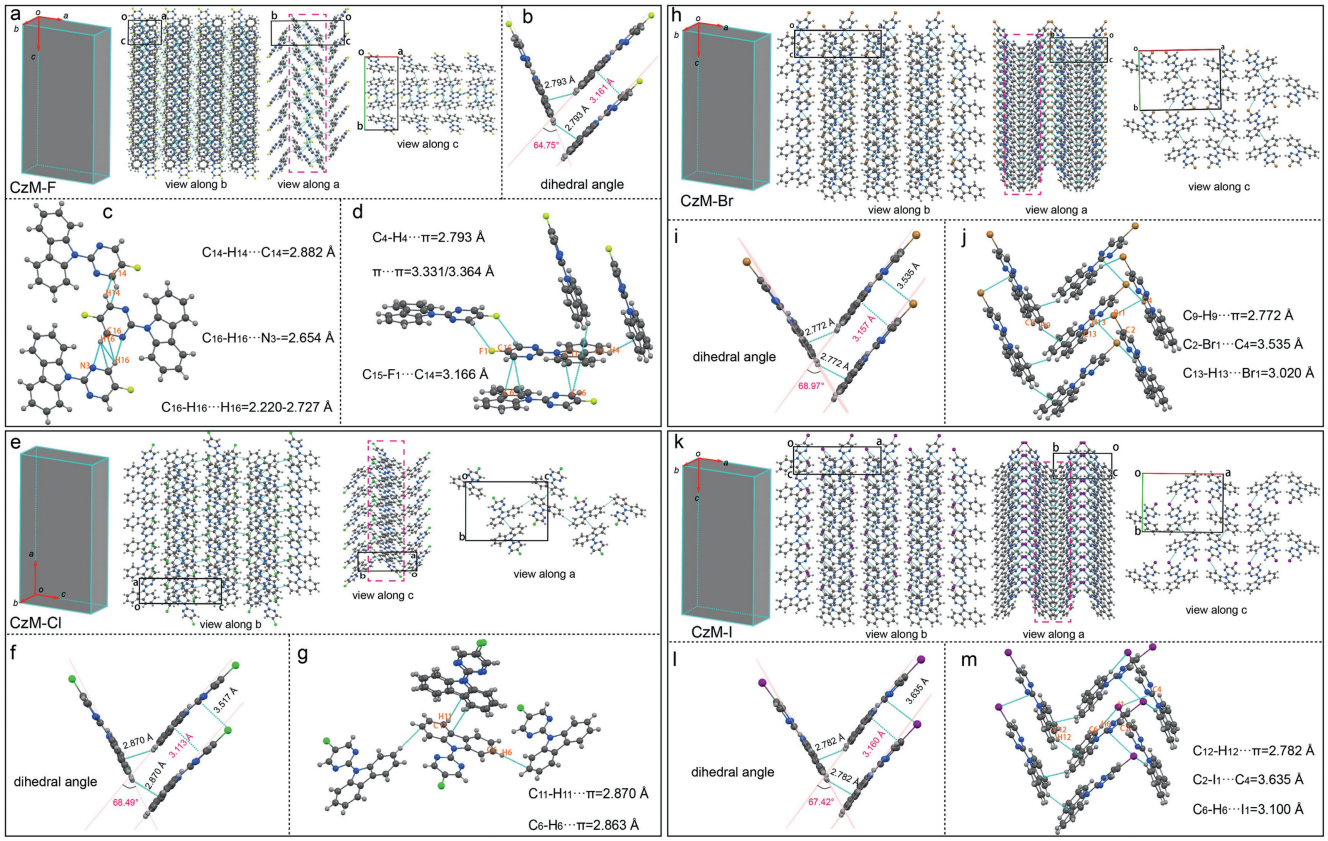

Fig. 3. Crystal structures of CzM-F, CzM-Cl, CzM-Br and CzM-I. (a-m) The schematic diagram related the macroscopic crystal model to molecular packing in the CzM-F (a), CzM-Cl (e), CzM-Br (h) and CzM-I (k) crystals with (c, d, f, g, i, j, l and m) detailed intermolecular interactions.

tions with a value of 3.161 Å (Fig. 3b). Meanwhile, it is easily observed a series of intermolecular non-covalent interactions, such as C_{16}-$H_{16}\cdots H_{16}$ = 2.220-2.727 Å, C_{16}-$H_{16}\cdots N_3$ = 2.654 Å, C_{14}-$H_{14}\cdots C_{14}$ = 2.882 Å, $\pi\cdots\pi$ = 3.331/3.364 Å (Figs. 3c and d). There is a stronger nucleophilic ability between F and C_{14} atom (C_{15}-$F_1\cdots C_{14}$ interaction, 5.060 Å) (Fig. 2a) than those of C_{13} atom (Figs. 2a and 3b–d, Fig. S16 in Supporting information). The CzM-Cl, CzM-Br and CzM-I crystals exhibited similar packing structures, but different from CzM-F. The molecules are stacked in parallel by intermolecular $\pi\cdots\pi$ interactions with a distance of 3.113 Å, 3.157 Å and 3.160 Å, respectively (Figs. 3f, i and l). There are a series of intermolecular interactions, including a small distance $C_8\cdots Cl_1$ (3.517 Å), C_{11}-$H_{11}\cdots\pi$ (2.870 Å), and C_6-$H_6\cdots\pi$ (2.863 Å) in Fig. 3g, C_2-$Br_1\cdots C_4$ (3.535 Å), C_9-$H_9\cdots\pi$ (2.772 Å), and C_{13}-$H_{13}\cdots Br_1$ (3.020 Å) in Fig. 3j, C_2-$I_1\cdots C_4$ (3.635 Å), C_{12}-$H_{12}\cdots\pi$ (2.782 Å) and C_6-$H_6\cdots I_1$ (3.100 Å) in Fig. 3m. Impressively, non-covalent interactions in other three crystals of CzM-Cl, CzM-Br and CzM-I, including a small distance $C_8\cdots Cl_1$, C_2-$Br_1\cdots C_4$, C_{13}-$H_{13}\cdots Br_1$, C_2-$I_1\cdots C_4$ and C_6-$H_6\cdots I_1$, were clearly distinct from the large distance between C_{13} and F_1 of CzM-F. This is due to the red region of halogen (Cl_1, Br_1 and I_1) with an access to interact with the blue region of the molecule (C_8 in CzM-Cl, C_4 and H_{13} in CzM-Br, C_4 and H_6 in CzM-I) (Figs. 2 and 3).

In general, the intermolecular interactions ultimately determine intermolecular packing model and style in the crystals. View along *a*-axis, CzM-F molecules show a "∧∨" packing structure with a dihedral angle of 64.75° that molecules are connected by C_4-$H_4\cdots\pi$. The "∧" parts and "∨" parts as a whole show a closely connection with $\pi\cdots\pi$ = 3.331/3.364 Å. Meanwhile, the "∧∨" packing structure along the *a*-axis is strongly connected by C_{16}-$H_{16}\cdots H_{16}$ = 2.220-2.727 Å, C_{16}-$H_{16}\cdots N_3$ = 2.654 Å, C_{14}-$H_{14}\cdots C_{14}$ = 2.882 Å, C_{15}-$F_1\cdots C_{14}$ = 3.166 Å. These intermolecular interactions are bad to form a slip plane parallel to (010) plane in CzM-F crystal, which is key to realizing intermolecular slipping (the red dotted line of Fig. 3a). From *c*-axis direction, similar to CzM-F crystal, CzM-Cl crystal also presents the "∧∨" packing structure connected by C_{11}-$H_{11}\cdots\pi$ interactions with a dihedral angle of 68.49°. However, "∧" packing structures are observed along (001) face, but the molecules exhibit "∨" packing model from the (002) plane. Besides, "∨∨" packing structure with the dihedral angles of the 68.97° and 67.42° is found for the CzM-Br and CzM-I crystals along the *a*-axis, which is linked by C_9-$H_9\cdots\pi$ and C_{12}-$H_{12}\cdots\pi$ interactions, respectively (Figs. 3i and l). More interestingly, the "∨" and "∨" packing structures joint in the same face linked by intermolecular interactions (C_2-$Br_1\cdots C_4$, C_{13}-$H_{13}\cdots Br_1$, C_2-$I_1\cdots C_4$ and C_6-$H_6\cdots I_1$). Similarly, the slip plane is (040) for CzM-Cl, (010) for CzM-Br, and (020) for CzM-I, respectively. Therefore, the monolayers were separated by Cl, Br and I atom (the red dotted line of Figs. 3e, h and k). The formation of slip plane is consistent with the result of electrostatic potential. The blue region of halogen atom (dotted line section around Cl, Br and I atoms) are absence of electrons and benefit for molecular slipping around slip plane (Fig. 2). Therefore, the surface of halogen atom with different electrostatic potential modulated the intermolecular interactions, which will create a nonnegligible impacts on the the crystal stacking and the huge change in mechanical properties.

The relationship between the macroscopic morphology and micro/nanostructure of the elastic crystal was established. The CzM-F crystal was broken (Fig. 1b) to investigate the surface morphology of the fracture section (Fig. S17 in Supporting information). There is smooth surface on the (010) and (100) faces. Meanwhile, lamellar structures observed on the fracture section also confirmed the

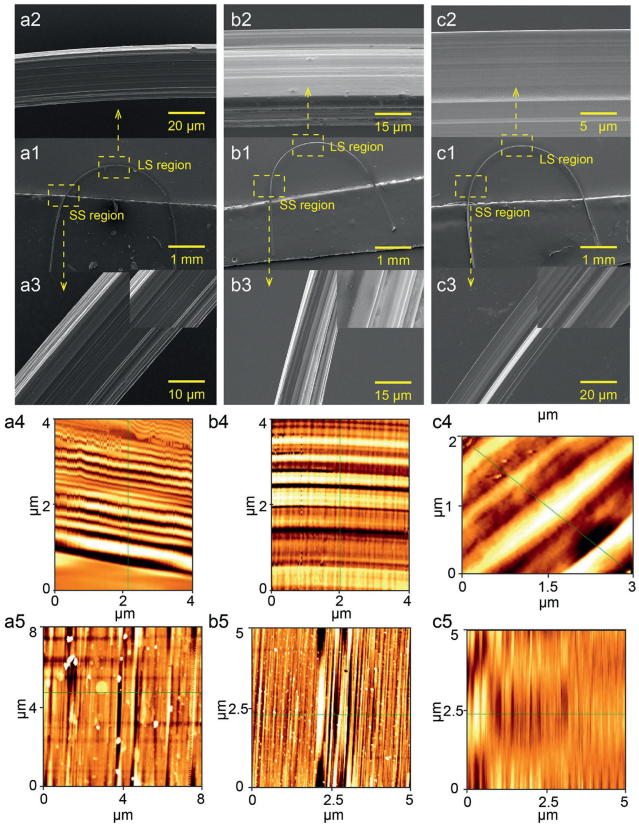

Fig. 4. SEM and AFM morphology of elastic crystals. (a) The (001) plane morphology of CzM-Cl bending crystal; a2 and a4 show the morphology in LS region; a3 and a5 show the morphology in SS region. The (100) plane morphology of (b) CzM-Br and (c) CzM-I bending crystal; b2 and b4 show the CzM-Br crystal morphology in LS region; b3 and b5 show the CzM-Br crystal morphology in SS region; c2 and c4 show the CzM-I crystal morphology in LS region; c3 and c5 show the CzM-I crystal morphology in SS region.

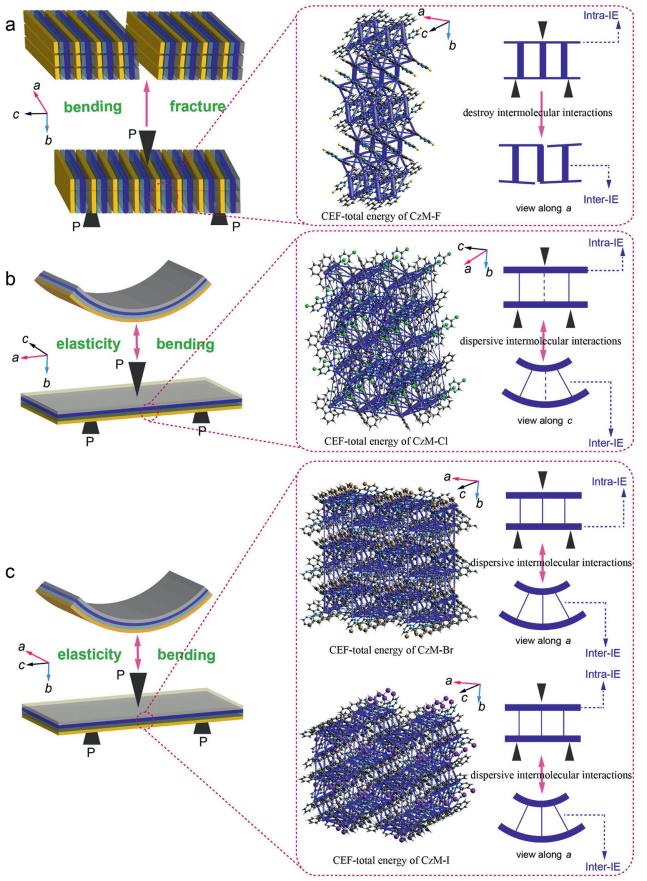

Fig. 5. Schematic representation of elastic bending of macroscopic crystals, CEFs for representing total IE (blue), and the consequences at microcosmic levels of structural change. (a) CzM-F, (b) CzM-Cl, (c) CzM-Br and CzM-I crystals.

crystals grew along the (001) plane. This surface morphology is markedly different from those of the other three elastic crystals. The large strain region (LS region) and small strain region (SS region) were carefully surveyed in the (001) plane for CzM-Cl and in the (100) plane for CzM-Br and CzM-I (Fig. 4). CzM-Cl crystals consisted of a series of lamellar nanosheets (Figs. 4a2 and 4a3). The bending face (010) is relatively smooth (Fig. S18a in Supporting information). Combined with the crystal growth morphology, the crystal grows along the long crystal axis and forms a thin lamellar structure in its thickness direction. Similarly, CzM-Br and CzM-I crystals also present a layered structural morphology on the (100) face. Besides, the surface morphology of the (010) bending surface shows a special smooth surface (Figs. S19b and c in Supporting information) attributed to more anisotropic intermolecular interactions. These slidable lamellar nanosheets are beneficial to realize energy absorption and release, which is precondition to obtain excellent elastic behavior. The distance and the depth of gullies between adjacent lamellar nanolayers in the LS and SS regions were explored by AFM. The thick lamella was observed in the LS region of the bent CzM-Cl crystal (Fig. 4a4). The interlayer distance was approximately 200–300 nm, and the depth of the interlayer gullies was approximately 100 nm (Fig. S20a2 in Supporting information). However, relatively dense thin-layer structures were observed at the SS region (Fig. 4a5). The interlayer distance reduced to about 5-100 nm, and the depth of interlayer gullies are also decreased to about 1–20 nm (Fig. S20a1 in Supporting information). Similar changes were observed for the CzM-Br and CzM-I elastic crystals (Fig. S20 in Supporting information). In general, the interlayer distance and gully depth in the LS region were larger than those in the SS region, due to the plastic deformation or plastic flow of the crystal under the micro/nanostructure state [20], which can also be confirmed by the typical loading pop-in phenomenon and the bending at the end point of the crystal (Figs. S11 and S18 in Supporting information). Two or more thin lamellar parts can be coupled to form a new thick lamellar structure owing to dense contact through plastic flow or deformation, which can also be confirmed by the abundant pop-in phenomena in nanoindentation.

In general, lamellar structures involved above in elastic crystal are the external manifestation of periodic intermolecular packing and arrangement in crystal, which is also called as molecular layers. Beyond the atomic-resolved structural perturbations, this reversible glide of preliminary periodic molecular layer is the fundamental parameter to ensure the bendable property of molecular crystal. Here, the introduced CEF analysis was successfully used to quantify the origin of brittleness of CzM-F and excellent elastic behavior of CzM-Cl, CzM-Br and CzM-I (see Supporting information for details). There are two key parameters need to be noted that the Intra-IE and Inter-IE, which may be defined as the minimum value of the cut-off energy within the slip molecular layer and maximum value of the cut-off energy between slip molecular layer, respectively. The crystal may break in case of the higher external energy than Intra-IE and Inter-IE. The quantified Inter/Intra-IE of organic molecular crystal will provide an insight into their mechanical behaviors. The electrostatic and dispersion energies of CzM-F show strong interaction energies along *b*-axis and weak along *a*-axis and *c*-axis, suggesting no obvious slip plane in CzM-F crystal (Fig. 5a and Fig. S21 in Supporting information). Mean-

while, it shows a weak Intra-IE in the *ac* plane and a strong Inter-IE in the *ab* plane for the CzM-F crystal (Fig. 5a). Therefore, it may initially break along *ac* plane rather than *ab* plane upon external force, attributed to the lower intermolecular interaction energy along *ac* plane (Fig. S25 in Supporting information). The discussion above also reasonably explained the brittle behavior of CzM-F. In contrary, CzM-Cl, CzM-Br and CzM-I crystals exhibited outstanding elasticity, associating with their excellent intermolecular noncovalent interactions and packing models. All three crystals present distinct lamellar structure with reversibly sliding behavior in the electrostatic, dispersion, and total energy frameworks (Figs. S22–S24 in Supporting information, Figs. 5b and c). The CzM-Cl crystal framework shows weak Inter-IE with low cut-off energy of 11.03 kJ/mol in the *b*-axis direction (such as the red shaded part in Fig. S26 in Supporting information). The lower interlayer binding energy enables the material to obtain a slip plane, which enables the molecule to move in a short range. The Intra-IE of 17.12 kJ/mol for CzM-Cl between the Cz units of adjacent molecules along the *c*-axis produces stronger interactions shown in the (010) bending plane. Besides, CzM-Br and CzM-I crystals show energy framework like CzM-Cl attributed to the similar lamellar structure. Their framework also shows a weak Inter-IE in the *b*-axis direction and a strong Intra-IE within the (010) bending plane. The Inter-IE is 18.47 kJ/mol for CzM-Br crystal and 16.48 kJ/mol for CzM-I crystal, which also shows a slide plane for the low interlayer binding energy (Figs. S27 and S28 in Supporting information).

Therefore, elastic molecular crystals always required the strong Intra-IE to prevent cleavage and the weak Inter-IE to ensure the short-range movement of molecules on the slip plane upon applied stress. The CzM-Cl crystals had a strong Intra-IE in the *ac* plane and a weak Inter-IE in *bc* plane. The crystal structures may maintain regular shape and ordered intermolecular arrangement but slight atomic-resolved structural perturbations and diffusion intermolecular interactions (Fig. 5b). The deformation of the elastic crystal also meets the unit cell elongation in the convex direction and contraction in the concave direction along the *a*-axis [27]. CzM-Br and CzM-I crystals both exhibited similar CEF properties to CzM-Cl but had a relatively higher Inter-IE (Figs. 5b and c). Based on previous studies [52], we also explore the structural changes of the crystal before and after bending to investigate the short-range movement of the internal molecules during bending. It can be found that the diffraction point of the straight crystal is sharp with a high intensity, owing to the uniform structure, while the diffraction peak of the bending crystal is weak and the diffraction point is diffused owing to the short-range molecular motion (Fig. S29 in Supporting information).

In this work, halo-pyrimidinyl Cz derivatives were systematically studied. The unique packing modes as the consequence of subtle difference of electrostatic potential lead to their distinguished elastic (CzM-Cl, CzM-Br and CzM-I) and brittle (CzM-F) behaviors when subjected to mechanical forces. SEM and AFM morphologies show that CzM-Cl, CzM-Br and CzM-I crystals possess lamellar micro/nanostructures. The CEF analysis provides sufficient clues for the reasonable Intra-IE and Inter-IE: (1) The strong interactions along the long axis of macroscopic crystal; (2) The relative strong interactions along the width of the macroscopic crystal representing the stronger Intra-IE; (3) Weak interactions along the direction of macroscopic crystal thickness representing the weaker Inter-IE. The stronger Intra-IE could prevent the cleavage of crystal and the weaker Inter-IE could ensure the short-range movement of molecules on the slip plane during bending. It is believed that this study gives a significant guideline for the functional design of halogen-based and/or Cz-based flexible crystals with potential photoelectric properties. The proposed Inter/Intra-IE theory can also be applied to explain the mechanical bendable mechanism of some crystals ever reported (HCB [52], DMS [41], PhOH-Cz and PhOM-Cz [35]).

Declaration of competing interest

The authors have no competing interests to declare that are relevant to the content of this article.

Acknowledgments

We acknowledge the primary financial support by the National Natural Science Foundation of China (No. 21975126), the open research fund from Anhui Province Key Laboratory of Optoelectronic Materials Science and Technology, and the Technology and Research Innovation in University of Jiangsu Province (No. KYCX21_0772), and the Ministry of Education and Synergetic Innovation Center for Organic Electronics and Information Displays.

Supplementary materials

Supplementary material associated with this article can be found, in the online version, at doi:10.1016/j.cclet.2022.107896.

References

[1] K. Wang, M.K. Mishra, C.C. Sun, Chem. Mater. 31 (2019) 1794–1799.
[2] P. Sanphui, M.K. Mishra, U. Ramamurty, et al., Mol. Pharm. 12 (2015) 889–897.
[3] G.R. Krishna, L. Shi, P.P. Bag, et al., Cryst. Growth Des. 15 (2015) 1827–1832.
[4] K. Naim, M. Singh, S. Sharma, et al., Chem. Eur. J. 26 (2020) 11979–11984.
[5] J. Peng, J. Bai, X. Cao, et al., Chem. Eur. J. 27 (2021) 16036–16042.
[6] M. Annadhasan, S. Basak, N. Chandrasekhar, et al., Adv. Opt. Mater. 8 (2020) 2000959.
[7] B. Liu, Q. Di, W. Liu, et al., J. Phys. Chem. Lett. 10 (2019) 1437–1442.
[8] H. Liu, Z. Lu, Z. Zhang, et al., Angew. Chem. Int. Ed. 57 (2018) 8448–8452.
[9] Y. Huang, Q. Gong, J. Yu, Sci. China Mater. 65 (2022) 1994–2016.
[10] R. Huang, C. Wang, Y. Wang, et al., Adv. Mater. 30 (2018) 1800814.
[11] X. Chu, Z. Lu, B. Tang, et al., J. Phys. Chem. Lett. 11 (2020) 5433–5438.
[12] H. Zhang, H. Liu, Z. Lu, et al., Angew. Chem. Int. Ed. 59 (2020) 12944–12950.
[13] S. Tang, K. Ye, H. Zhang, Angew. Chem. Int. Ed. (2022) 202210128.
[14] X. Yang, L. Lan, L. Li, et al., Nat. Commun. 13 (2022) 2322.
[15] L. Lan, L. Li, Q. Di, et al., Adv. Mater. 34 (2022) 2200471.
[16] L. Lan, X. Yang, B. Tang, et al., Angew. Chem. Int. Ed. 61 (2022) e202200196.
[17] Y. Liu, P. Yang, K. Zhang, et al., Cryst. Growth Des. 22 (2022) 1312–1318.
[18] S. Hayashi, S.Y. Yamamoto, D. Takeuchi, et al., Angew. Chem. Int. Ed. 57 (2018) 17002–17008.
[19] K. Huang, L. Song, K. Liu, et al., NPJ Flex. Electron. 5 (2021) 21.
[20] M. Annadhasan, A.R. Agrawal, S. Bhunia, et al., Angew. Chem. Int. Ed. 59 (2020) 13852–13858.
[21] B. Bhattacharya, D. Roy, S. Dey, et al., Angew. Chem. Int. Ed. 59 (2020) 19878–19883.
[22] Y. Chen, Z. Chang, J. Zhang, et al., Angew. Chem. Int. Ed. 60 (2021) 22424–22431.
[23] M. Owczarek, K.A. Hujsak, D.P. Ferris, et al., Nat. Commun. 7 (2016) 13108.
[24] M.S. Kazantsev, V.G. Konstantinov, D.I. Dominskiy, et al., Synth. Met. 232 (2017) 60–65.
[25] S.K. Park, H. Sun, H. Chung, et al., Angew. Chem. Int. Ed. 59 (2020) 13004–13012.
[26] A. Worthy, A. Grosjean, M.C. Pfrunder, et al., Nat. Chem. 10 (2018) 65–69.
[27] A.J. Thompson, A.I. Chamorro Orué, A.J. Nair, et al., Chem. Soc. Rev. 50 (2021) 11725–11740.
[28] J.S. Geng, L. Mei, Y.Y. Liang, et al., Nat. Commun. 13 (2022) 2030.
[29] S. Iamsaard, S.J. Aßhoff, B. Matt, et al., Nat. Chem. 6 (2014) 229–235.
[30] J. Cao, H. Liu, H. Zhang, CCS Chem. 3 (2021) 2569–2575.
[31] S. Ghosh, M.K. Mishra, S. Ganguly, et al., J. Am. Chem. Soc. 137 (2015) 9912–9921.
[32] T.-R. Wei, M. Jin, Y. Wang, et al., Science 369 (2020) 542–545.
[33] X. Shi, H. Chen, F. Hao, et al., Nat. Mater. 17 (2018) 421–426.
[34] K. Tang, W. Qi, Y. Wei, et al., Research 2022 (2022) 9765121.
[35] C. Wei, L. Bai, X. An, et al., Chem 8 (2022) 1427–1441.
[36] L. Adler-Abramovich, Z.A. Arnon, X. Sui, et al., Adv. Mater. 30 (2018) 1704551.
[37] D. Lin, J.A. Liu, H. Zhang, et al., Adv. Mater. 34 (2022) 2109399.
[38] S. Ghosh, C.M. Reddy, Angew. Chem. Int. Ed. 51 (2012) 10319–10323.
[39] C.M. Reddy, M.T. Kirchner, R.C. Gundakaram, et al., Chem. Eur. J. 12 (2006) 2222–2234.
[40] S. Ghosh, M.K. Mishra, S.B. Kadambi, et al., Angew. Chem. Int. Ed. 54 (2015) 2674–2678.
[41] S.P. Thomas, M.W. Shi, G.A. Koutsantonis, et al., Angew. Chem. Int. Ed. 56 (2017) 8468–8472.
[42] S. Saha, G.R. Desiraju, J. Am. Chem. Soc. 139 (2017) 1975–1983.

[43] A. Mondal, B. Bhattacharya, S. Das, et al., Angew. Chem. Int. Ed. 59 (2020) 10971–10980.
[44] J.R. Wang, M. Li, Q. Yu, et al., Chem. Commun. 55 (2019) 8532–8535.
[45] C. Wang, C.C. Sun, Mol. Pharm. 16 (2019) 1732–1741.
[46] C.M. Reddy, K.A. Padmanabhan, G. Desiraju, Cryst. Growth Des. 6 (2006) 2720–2731.
[47] S. Saha, G. Desiraju, J. Am. Chem. Soc. 139 (2017) 1975–1983.
[48] S. Ghosh, C.Malla Reddy, CrystEngComm 14 (2012) 2444–2453.
[49] P.R. Spackman, M.J. Turner, J.J. McKinnon, et al., J. Appl. Crystallogr. 54 (2021) 1006–1011.
[50] L. Wang, N. Liu, B. Dai, RSC Adv. 5 (2015) 82097–82111.
[51] D. Tu, J. Zhang, Y. Zhang, et al., J. Am. Chem. Soc. 143 (2021) 11820–11827.
[52] M.K. Panda, S. Ghosh, N. Yasuda, et al., Nat. Chem. 7 (2014) 65–72.